Water-Mediated Formation of Hydride Derivates from Flexible Pd-Salan Complexes: A DFT Study

Mihály Purgel,[*,†] *Péter Pál Fehér,*[‡] *Álex Kálmán Balogh,*[†,#] *Szilvia Bunda,*[†,#] *and Ferenc Joó*[†,§]

[†]Department of Physical Chemistry, University of Debrecen, Egyetem tér 1, H-4032 Debrecen, Hungary

[‡]Research Centre for Natural Sciences, Magyar tudósok körútja 2, H-1117 Budapest, Hungary

[#]Doctoral School of Chemistry, University of Debrecen, P.O.Box 400, Debrecen, H-4002 Hungary

[§]MTA-DE Homogeneous Catalysis and Reaction Mechanisms Research Group, University of Debrecen, Egyetem tér 1, H-4032 Debrecen, Hungary

Abstract

The formation of hydride derivatives of sulfonated palladium(II) salan (hydrogenated salen) complexes was studied with DFT methods. The non-hydrolytic property, chirality, and flexibility lead to a significant difference compared to salen derivatives. We made a detailed computational study to understand the relevance of the flexibility in contrast to the rigid salen complex. Two main pathways were investigated: one of them was a direct monohydride formation where the oxygen of the phenolate group was substituted by a hydrogen molecule followed by a proton transfer. Another was an indirect monohydride formation involving the substitution of phenolate arm by a solvent water molecule in the first step and subsequent reaction with H_2 in the second. We focused on weak interactions among the Pd-complex and water molecules. Trigonal, square, and diamond motifs of H-bond networks were found around

the oxygen atom of the phenolate arm which is crucial during the proton transfer step, however, substitution steps prefer chain type motifs.

Keywords: hydrogen, density functional theory, mechanism, catalyst, hydride, water-soluble, sulfonate group

1. Introduction

Schiff base catalysts such as salen complexes are commonly employed in various reactions. First-row transition metal centers are established in enantioselective organic synthesis, electrocatalytic or enzymatic processes [1-6], antiviral agents [7], and oxidants [8,9]. Meanwhile, heavier metal ions offer exceptional performance in C−C coupling and hydrogenation reactions [10–14]. Regardless of the choice of the metal, the chelate rings containing the imine groups have an intrinsic rigidity that further influences the reactivity at the metal center via steric strain. This can be exploited by tuning the flexibility of the ligand through modifications at the ethylene backbone or simply hydrogenating the imine groups to amines, as shown in Fig. 1. The latter approach yields the salan (tetrahydrosalen) ligands which offer improved hydrolytic stability over the salen analogs, a crucial property in aqueous applications. Sulfonation of the phenyl rings yields water-soluble palladium(II)-sulfosalen (SS), and sulfosalan (HSS)-type catalysts which our group has successfully applied in hydrogenation, redox isomerization, and C–C coupling reactions [15–18]. It is generally accepted that salan complexes are more flexible than the corresponding salens due to the sp^3 nitrogen atoms, but whether this introduces more favorable reaction channels in the mechanisms remains to be elucidated [26,27]. Therefore, to gain a deeper understanding, we used DFT to study the reaction of PdHSS with molecular hydrogen that yields hydride complexes. By accounting for

the different isomers of PdHSS, the effect of ligand flexibility is explained in terms of conformational changes that may depend on the solvent arrangement.

In a previous study about redox isomerization of allylic alcohols, we identified a potentially active catalytic hydride species which contains a dissociated phenol subunit [15]. We proposed that it is an intermediate of the dehydrogenation cycle and is produced *via* a simultaneous hydride and proton transfer to the Pd center and the phenolate oxygen in the HSS ligand. Therefore, the reaction most likely requires an internal rotation of the phenolate arm in some way. We limit the discussion to the hydride formation process as this reaction step itself exhibits all the complexity of the conformational behavior. We also discuss potential structural modifications of the ligand and how these can lead to different energetics *via* steric and electronic effects. Substituted salen and salan derivatives are well known in the literature forming complexes with different metals [19,20]. Cytotoxic activity and various enantioselective oxidation or epoxidation reactions have been investigated by asymmetric *ortho*-, *para*-substituted, and half reduced derivatives [21–24]. The methoxy-substituted Pd-salan complex can even form a multinuclear complex with samarium and can be used to catalyze asymmetric Friedel–Crafts reactions [25].

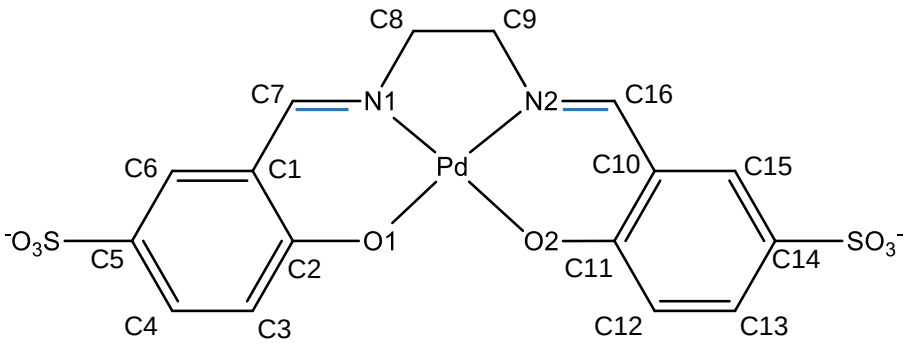

Figure 1. The numbering of atoms of PdSS (blue bonds refer to imine groups) and PdHSS (all black bonds).

2. Computational details

The DFT calculations [28] were carried out using the Gaussian09 software package [29]. Geometry optimizations were performed with the M06 functional [30]. The Def2TZVP ECP/basis set was employed on palladium [31], together with the TZVP basis set for non-metal atoms [32,33]. Frequency calculations were done at the level of the theory of geometry optimization. Relative free energies (ΔG) are reported at 298.15 K and atmospheric pressure. The solvent (water) effect was accounted for the Polarized Continuum Model (IEF-PCM) [34] as an implicit solvent model, but explicit water molecules were also taken into account. All the energies were calculated relative to the [ML + 2 H_2O + H_2] adduct reference state. All stationary points were confirmed by frequency analysis where minima had all positive frequencies and TSs had one imaginary frequency related to the actual movement of the reaction coordinate.

3. Results and discussion

3.1. Flexibility, isomers and conformers of PdSS and PdHSS complexes

PdSS and PdHSS complexes contain a central five-membered chelate ring with a nonplanar ethylene backbone breaking the C_{2v} symmetry of the simplified representation in Fig. 1. This introduces λ and δ helical conformers [35] which may interconvert *via* ethylene inversion (EI) as shown in Fig. 2. PdSS has a much lower EI barrier than PdHSS isomers, but both complexes can transform into the delta (inverted) form. The saturation of imine groups to amines yields two nitrogen stereocenters in PdHSS, giving rise to (R,R) – (S,S) and (R,S) – (S,R) enantiomeric pairs (Fig. S1). For a detailed structural analysis see the Supplementary Material.

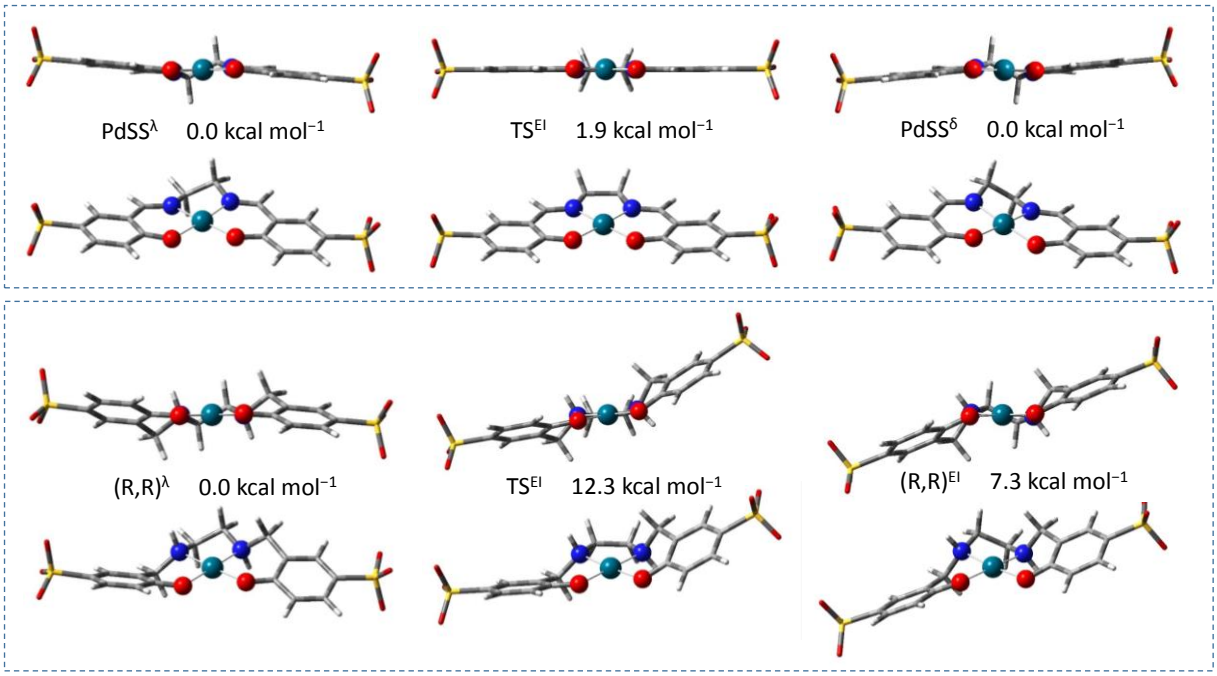

Figure 2. The λ and δ helical isomers of the PdSS and (R,R) diastereomer of PdHSS in different orientations. Palladium, nitrogen, and oxygen atoms are indicated as grey, blue and red spheres, respectively, while a tube representation is used for the rest of the molecule.

The sp^3 methylene carbon between the amino nitrogen and the phenolic ring in the PdHSS complex is partially responsible for the flexibility of phenolate arms. The most stable $(R,R)^{\lambda}$ or simply (R,R) conformer is the closest to being planar; the two phenolic rings are roughly parallel to the coordination plane. From this position, internal rotation (arm rotation) can set the rings to an almost perpendicular orientation relative to the central chelate ring, as shown in Fig. 3. These are denoted as half stepped (hs) or stepped (s) conformations depending on whether only one or both rings are rotated. Such conformers of the salen complexes have already been characterized by others [36,37]. Previously, we proposed that the half stepped conformer of the (R,R) isomer is relevant in a concerted hydrogen activation process (simultaneous hydride and proton transfer) where the planarity of the complex is broken by arm rotation [15].

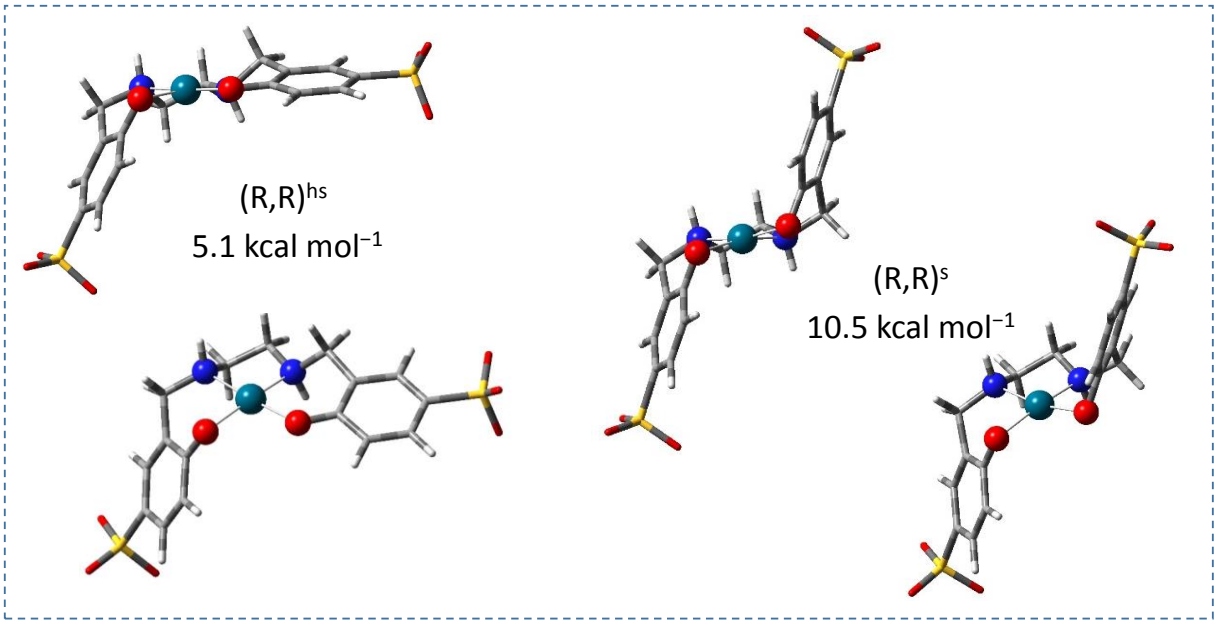

Figure 3. The internal arm rotated (half stepped and stepped) conformers of the PdHSS in different orientations.

3.2. Hydride formation: general considerations

As the (R,R) conformer with two equatorial phenolate arms is the most stable PdHSS diastereomer, we firstly investigated the formation of the catalytically active hydride species from this structure. The process requires H_2 uptake and may take place *via* two main pathways. Direct hydride formation starts with the substitution of the phenolate group by a hydrogen molecule. It is then followed by the heterolytic dissociation of the hydrogen to yield a metal hydride and a phenol via proton transfer to the dissociated phenolate. The other, indirect pathway involves an initial replacement by water with subsequent water–hydrogen exchange and proton transfer steps. Depending on the direction of H_2 or H_2O coordination, the phenolate arm may move towards the hydrogen of the proximal amino group as well in the opposite direction, as shown in Fig. 4. To model this process better, we included two additional explicit water molecules that stabilize the negatively charged, dissociated phenolate group (Fig. S7). The numerous hydrogen bond donor and acceptor groups create a large system of hydrogen bonds that give rise to many motifs throughout the mechanism of the hydride formation. Note

that we could not find a minimum in which hydrogen is coordinated to the axial site as expected from the d^8 electron configuration of palladium(II).

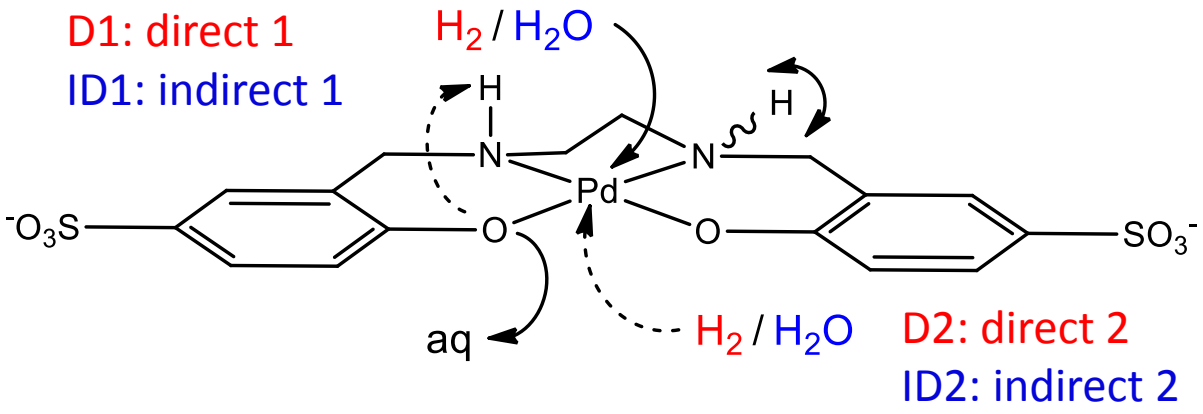

Figure 4. Orientation of the coordinating small molecules relative to the complex. Black arrows are representing the D1 and ID1 processes while dashed arrows sign the D2 and ID2 ones.

3.3. Pd-H formation: Direct route - the D1 mechanism

D1 denotes the pathway where the phenolate arm is turned opposite to the –NH group. Upon H_2 coordination, the two added water molecules and the dissociated phenolate oxygen (O1) can form a trigonal hydrogen bond network (▲). This substructure then remains a common pattern in all the intermediates and transition states of this pathway, as shown in Scheme 1. One of the water molecules (W1) is also hydrogen-bonded with the hydrogen of the distant amino group on the N2 atom (H^{N2}) while the other one (W2) is bonded to the coordinated oxygen of the other phenolate group (O2) as well.

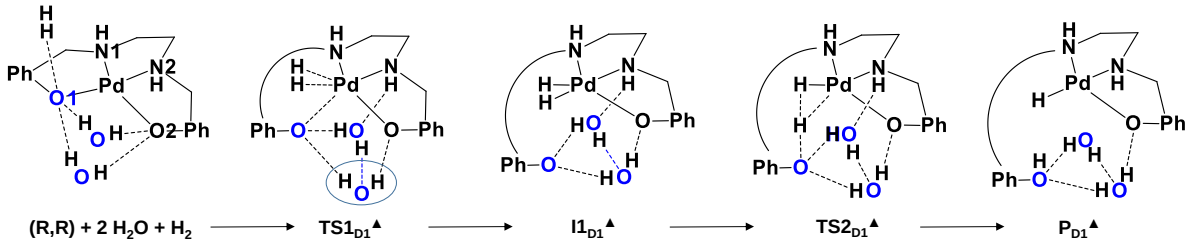

Scheme 1. Trigonal hydrogen bond network in the most relevant species of (R,R) isomer in the D1 mechanism. Additional H-bonds are represented by blue dashed lines, the distal amino group is by purple. The water surrounded by ellipsoid is the W2 mentioned in the text.

Hydrogen coordination may also take place without the trigonal bond network; in $TS1_{D1}$ (at 19.2 kcal mol^{-1}) the two water molecules are disconnected, but they still provide more stabilization compared to the trigonal $TS1_{D1}^{\blacktriangle}$ (at 20.3 kcal mol^{-1}). The corresponding $I1_{D1}$ is also lower in energy than $I1_{D1}^{\blacktriangle}$ (16.7 vs. 19.2 kcal mol^{-1}), however, they both lead to the same trigonal $TS2_{D1}^{\blacktriangle}$ of proton transfer at 20.0 kcal mol^{-1}. This indicates that the trigonal motif not only makes the dissociated phenolate arm more stable but is also required in the proton transfer step of the D1 mechanism. Note that in the non-trigonal $TS1_{D1}$ the $O^{W1}\cdots H^{N2}$ H-bond is much shorter than in the trigonal $TS1_{D1}^{\blacktriangle}$ (216 vs. 259 pm). The difference is less apparent in the corresponding I1 states where the bond distances are 193 vs. 202 pm. In terms of energy, however, $I1_{D1}$ is more stabilized than $TS1_{D1}$ relative to their trigonal analogs. This indicates that the trigonal H-bond network causes a larger strain in the TS.

We explored additional I1 forms and found one where the dissociated phenolate arm is further away from its original position. In these structures, the sulfonate group at the para position may interact with the coordinated hydrogen through a water molecule (Fig. S8). The protonation of the sulfonate group, however, yields an inferior hydride state (7.2 kcal mol^{-1}). From a slightly different I1 conformation, the phenolate may get protonated via a water channel, but this pathway is kinetically non-competitive ($TS2_{D1}^{W}$ at 26.2 kcal mol^{-1}).

The results are collected in Table 1, which also shows the calculated energies for the equivalent states corresponding to the EI isomer. Among these, only $I1_{D1}^{EI\blacktriangle}$ and $TS2_{D1}^{EI,W}$ are lower in energy than their (R,R) counterparts, probably because the water molecule bonded to H^{N2} changes the Pd–N2–H angle slightly (from +106º to +103º vs. +102º/+101º).

As previously mentioned, the (R,R) diastereomer has additional half stepped and stepped conformers. Although the corresponding reactant states lie higher in energy, the phenolate arm is in a more favorable orientation for the D1 mechanism. This is reflected by the activation barriers of both main steps as they provide the lowest values out of all the considered scenarios so far. $TS1_{D1}^{hs}$ contains a similar H-bond network to the $TS1_{D1}$, however, there is another H-bond network in which the trigonal structure is broken not between the water molecules but rather at the $O1\cdots H^{W1}$ bond, as shown in Fig. 4. This $TS1_{D1}^{hs}$* state provides the most favorable H_2 coordination ($TS1_{D1}^{hs}$*) with 18.1 kcal mol^{-1}, and even leads to the final hydride product through a coupled proton transfer. Note that from $I1_{D1}^{hs}$ a spontaneous H-bond reorientation occurred during proton transfer similar to the one in $TS1_{D1}^{hs}$*. Moreover, the products of these pathways (P_{D1}^{hs} and P_{D1}^{hs}*) are the most stable stationary points in the direct mechanisms (-2.0 kcal mol^{-1}). Arm rotation and ethylene inversion together shift one water between H^{N2} and sulfonate group to build H-bonds with them, see Fig. S9. Note that these products can interconvert each other, however, we did not study this.

Table 1. Relative energies in kcal mol^{-1} of the stationary points of the direct mechanisms for the (R,R) isomer of the PdHSS complex.

	(R,R)	$(R,R)^{EI}$
$TS1_{D1}$	**19.2**	**23.0**
$TS1_{D1}$▲	**20.3**	**23.6**
$TS1_{D1}^{hs}$	**20.7**	**20.7**
$TS1_{D1}^{hs}$*	**18.1**⁂	**24.6**
$TS1_{D2}$	**24.5**	**34.7**
$I1_{D1}$	16.7	17.6
$I1_{D1}$▲	19.2	18.4
$I1_{D1}^{W}$	19.5	19.8
$I1_{D1}^{hs}$	17.8^{Hr}	18.6
$I1_{D2}$	18.2	–
$I1_{D2}^{W}$	17.5	21.2
$TS2_{D1}$▲	**20.0**	**22.7**
$TS2_{D1}^{W}$	**26.2**	**24.5**
$TS2_{D1}^{hs}$	–	**18.5**
$TS2_{D2}$	**20.5**	**24.2**

$TS2_{D2}{}^{W}$	**25.0**	**27.7**
P_{D1}	1.6	-0.4▲
$P_{D1}{}^{W}$	-1.1	-1.8
$P_{D1}{}^{hs}$	-2.0	-0.04
P_{D2}	3.3	5.5^{D1}
$P_{D2}{}^{W}$	2.7	4.7

[*] concerted process
[Hr] spontaneous H-bond reorientation causes concerted proton transfer → no $TS2_{D1}{}^{hs}$
[D1] D1 type product
[n.c.] not calculated

3.4. Pd-H formation: Direct route - the D2 mechanism

In the D2 mechanism, the arriving hydrogen molecule displaces the phenolate arm towards the proton of the proximal amino group of the N1 atom. After H_2 coordination (in $I1_{D2}$), these water molecules move between the amino group and O1. From there, two pathways are available: one water can be inserted between O1 and H^P to initiate a proton transfer *via* a water channel, or the water can move further away to make a direct proton transfer to the phenolate oxygen possible. The latter is the preferred pathway over the water-assisted one (20.5 vs. 25.0 kcal mol^{-1}), see Scheme S1. This result is very similar to the conclusion of the D1 mechanism (Table 1) as both prefer the direct proton transfer. Considering EI, a significant difference was found energetically between $TS1_{D2}$ and $TS1_{D2}{}^{EI}$ (24.5 and 34.7 kcal mol^{-1}, respectively), which is likely due to the distortion of the square planar ligand environment. In the case of $TS1_{D2}{}^{EI}$, the *trans* N1 and O2 atoms can no longer be considered collinear with the Pd center; the N1–Pd–O2 angle changes from 173º ($TS1_{D2}$) to 167º. We also identified an apical intermediate I1D2^ (Fig. S10) at 18.8 kcal mol^{-1} in which the coordinated hydrogen molecule is almost parallel to the coordination plane i.e. perpendicular to the phenyl ring of the dissociated phenolate.

3.5. Comparing direct routes: D1 vs. D2 mechanism

In (R,R) the dihedral angles (β_1: Pd–N1–C1–C7, β_2: N1–C1–C7–C2 and β_3: C1–C7–C2–O1) of phenolate arm involving the Pd–N1–C1–C7–C2–O1 unit were 67°, -53° and 2°. In the D1

pathway, two of these dihedral angles change significantly: 54°, -72° and 5° in $TS1_{D1}$ and 45°, -91° and 0° in $I1_{D1}$, while in the D2 pathway only β_2 changed considerably: 67°, -7° and 0° in $TS1_{D2}$ and 60°, 51° and 2° in $I1_{D2}$. However, a simple fictive protonation of (R,R) resulted in values of 69°, -59° and 0° where β_2 changed the most (-6°), and went to the D1 direction presuming the preference of D1, see Table 2. Differences of dihedral angles (Δ_i) and the sum of the absolute values of β_i and Δ_i shows that $TS1_{D1}$ is more appropriate than $TS1_{D2}$, especially when they are compared to the protonated species H[(R,R)]. $\sum|\beta_i|$ is much less for $TS1_{D2}$ than for other species, while Δ_1 and Δ_3 (differences referred to $TS1_{D1}$) are smaller than Δ_2 and Δ_4 (differences referred to $TS1_{D2}$).

Table 2. Dihedral angles of the (R,R), its protonated form, the two TS1 of direct mechanisms, and the differences where Δ_1 = (R,R) - $TS1_{D1}$, Δ_2 = (R,R) - $TS1_{D2}$, Δ_3 = H[(R,R)] - $TS1_{D1}$, Δ_4 = H[(R,R)] - $TS1_{D2}$.

	(R,R)	**H[(R,R)]**	**$TS1_{D1}$**	**$TS1_{D2}$**	Δ_1	Δ_2	Δ_3	Δ_4
β_1	67	69	54	67	13	0	15	2
β_2	-53	-59	-72	-7	19	-46	13	-52
β_3	2	0	5	0	-3	2	-5	0
$\sum\|\beta_i\|$ or $\sum\|\Delta_i\|$	**122**	**128**	**131**	**74**	*35*	*48*	*33*	*54*

The disadvantage of the D2 mechanism can be also observed by the endergonic character of the process in which hydride products (P_{D2} and P_{D2}^{W}) have less favored orientations than in products of D1 mechanism (P_{D1}^{hs}*, P_{D1} and P_{D1}^{W}). On the other hand, these forms can interconvert each other. The most relevant structures of D1 and D2 mechanisms are represented in Fig. 5 and Fig. S11, respectively.

The monohydride formation affects the other bonds in the coordination sphere: the initial Pd–N1, Pd–N2, and Pd–O2 bond distances are longer in the product state by approximately 5, 12, and 3 pm, respectively (Table S9). We also found an inferior monohydride product complex at

19.6 kcal mol^{-1} with a different coordination environment (Fig. S12). In this isomer, one of the amino groups is substituted instead of the phenolate. Due to the higher energies of the (R,S) species, see Table S2, mechanisms of the less stable (R,S) isomer are discussed in SI in detail. It is worth mentioning that we found transition states without explicit water molecules as well but those are typically 4-5 kcal mol^{-1} higher in energy, see Table S5. Additionally, from the I1 structures, we explored pathways that involve dihydride complex formation and H-transfer to the C1 atom. These are discussed in the Supplementary Material in more detail as all of them involve high energy intermediates like Pd(IV) complexes.

The relevance of the monohydride species was also proven by experimental methods (^{1}H NMR and UV-Vis spectroscopies) and simulated spectra, which were in good agreement (see details in the Experimental section of the Supplementary Material). Based on all these data, we can conclude that the catalytically active species is a monohydride complex.

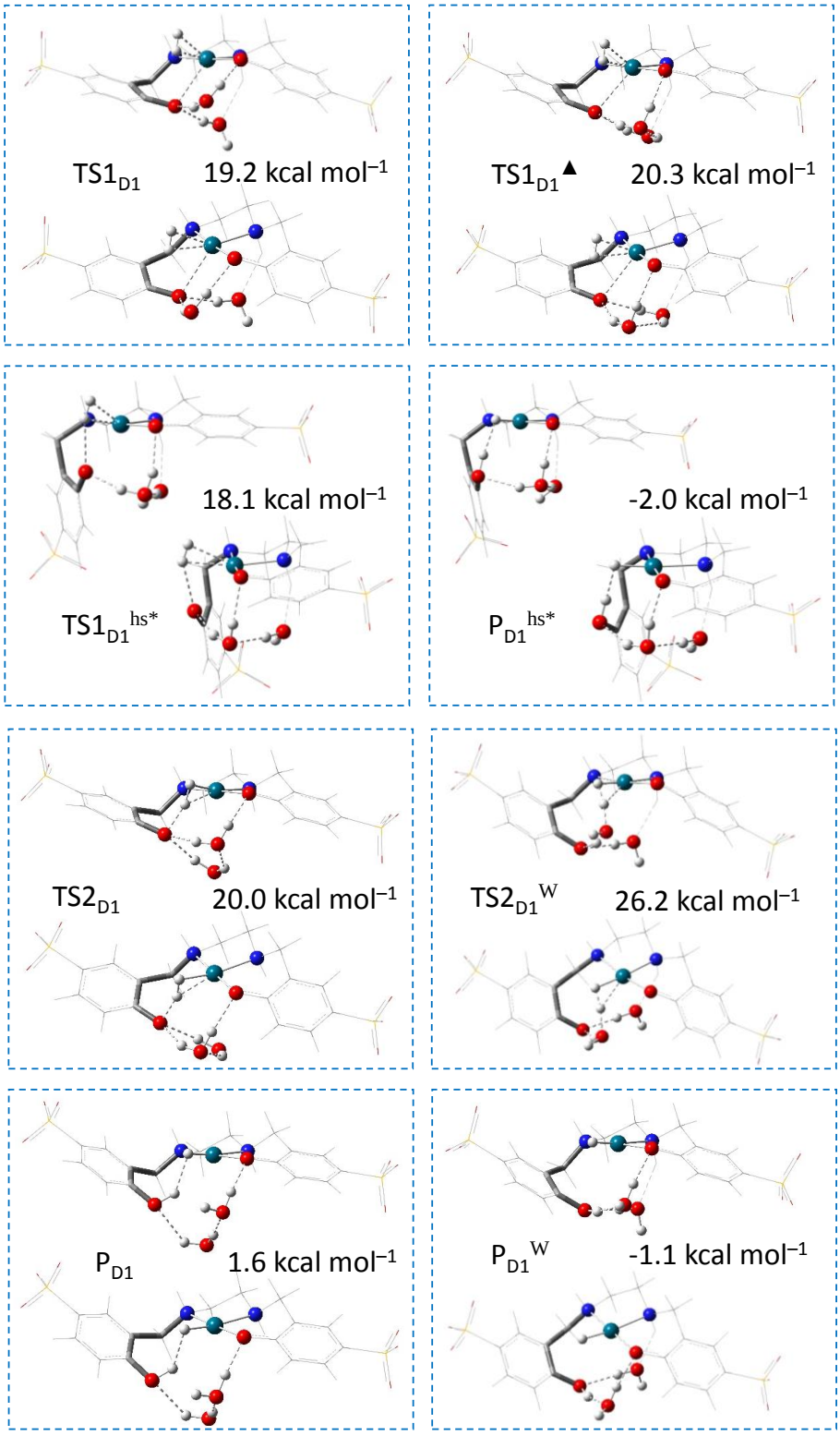

Figure 5. The most relevant stationary points of the D1 mechanisms in different orientations. Palladium is grey, nitrogen is blue, oxygen is red, hydrogen is white, the tube represents the relevant dissociating phenolate arm, and the wireframe shows the rest of the molecule.

3.6. Further rearrangements of the hydride product

We performed calculations for species involving one coordinated water molecule in the place of the amino group of the hydride products. Without the coordinated N1 atom, the Pd has a half coordinated salan ligand and the two other sites are filled by a hydride and a water molecule as shown in Fig. 6. Unfortunately, the TS of the substitution between the water and the amino group (25.5 kcal mol^{-1}) was found only without second water in the outer sphere, see Fig. S27. It can be seen that the position of the non-coordinating water molecule affects strongly the energy of the species. We also studied the proton transfer from the coordinated water to the free amino group resulting in a complex having both hydride and hydroxide ligands (P3). In P4, however, proton transfer was studied between the dissociated amino group and the dissociated phenolate oxygen where P5 has a zwitterion salan ligand. Zwitterion forms can be only stabilized by water molecules while without them proton transfer occurred from the NH_2^+ groups to the phenolate oxygens. We also found that in P4 or P5 the hydride ligand can be transferred from the palladium to the coordinated nitrogen (N2) as a proton. This yields P6 and P7, which contain a palladium(0) center and another zwitterion ligand coordinated weakly to the neutral metal by O2 atom, see Fig. 6. The reduction of the metal ion is confirmed by APT charges which showed +0.107 and +0.096 values for P6 and P7, respectively. Note that typical APT values are more positive in the previously introduced complexes: e.g. in (R,R) was +1.510, in $I1_{D1}$ was +1.017 while in P2 was +1.027, and in P4 was +1.054. We investigated whether the hydride can be transferred to the coordinated phenolate O2 instead of N2. The obtained P8 complex also contains a Pd(0) center with APT charge of +0.114 together with a weakly coordinated salan. In this case, however, the ligand coordinates only through its N2 atom as the "second" protonated phenolate arm dissociates. Without water molecules, the analogous direct H-transfer to O2 has an activation barrier of 36.2 kcal mol^{-1} and the product has energy (18.5 kcal mol^{-1}) similar to that of P8 (17.3 kcal mol^{-1}), see Fig. S28. The relatively high energies of

species including water in the inner coordination sphere, or having Pd(0) can be relevant in that case when the activation barrier of a given reaction is over these energies. The dimerization of the Pd0 species was also studied, and we found that different orientations of dimers can occur which are thermodynamically very favored, see Fig. S29. In dimers, Pd–Pd bonds were formed with 263 and 266 pm distances which are very similar to the one found in a simple linear trimer Pd(0) chain (266 pm). Previous *ab initio* calculations report an equilibrium Pd–Pd distance in a palladium wire at around 250 pm, however, interatomic distances are in a wide range (240–300 pm) [38–40]. On the other hand, the experimental bulk distance was found at 267 pm which is in good agreement with our result [40]. We found that at higher concentration (35 mM) a dark ring of a precipitate appeared on the wall of the NMR tube while the deep yellow color of the solution became pale yellow in the case of 5 bar hydrogen pressure. We could not see similar precipitation in other cases e.g. at a lower concentration or lower H_2 pressure, or in the presence of substrate.

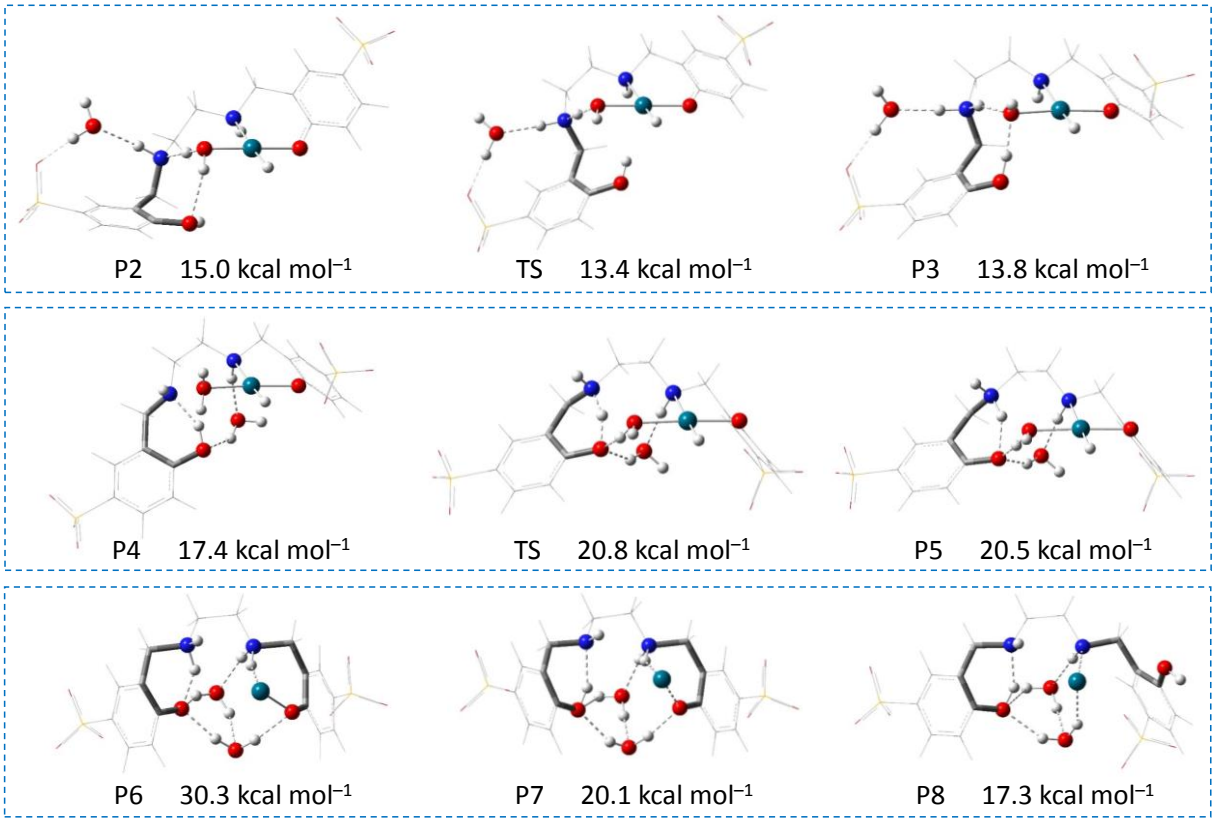

Figure 6. Optimized structures of proton transfers having coordinated water molecule in hydride products (upper and middle sections), and complexes including palladium(0) (bottom section).

3.7. Pd-H formation: Indirect route – the ID1 mechanism

The indirect mechanism involves a preliminary phenolate–water substitution ($TS1_{ID}$) before the hydrogen coordination ($TS2_{ID}$) and proton transfer ($TS3_{ID}$) steps. The key difference here is that the Pd−O1 bond is already dissociated when the hydrogen appears. Note that in the R_{ID} reactant state the orientation of the loosely bound H_2 is somewhat different from R_D, see Fig. S7. The main difference between the two reference states is that R_{ID} includes an additional water molecule as a reactant. In the ID1 approach, the corresponding TS1 structures contain two main patterns which were formed during the geometry optimization: the one in $TS1_{ID1}$▲■ consists of a trigonal motif built by O1, $O^{W1,}$ and O^{W2} together with a square shape built by O1, O2, and two water oxygens. The other arrangement is energetically more preferred and has a chain formed by O1 and the three water oxygens in $TS1_{ID1}$, see Fig. S30. Note that square motif means that atoms in a projection show square shape but those are not in a plane.

Both $TS1_{ID1}$ and the arm rotated $TS1_{ID1}{}^{hs}$ as well as the related intermediates are lower in energy than their D1 equivalents indicating a favored phenolate–water substitution. The relevant energies are collected in Table 3. In the stationary points of the subsequent reaction steps ($TS2_{ID1}$, $I2_{ID1}$, $TS3_{ID1}$) only the trigonal motif (▲) remains while the square unit breaks up. This arrangement then changes again in the monohydride product (P_{ID1}), where the dissociated water moves into the trigonal region to yield a square pattern of oxygen atoms (■). This pathway is less preferred than its D1 counterpart which creates a more complicated situation among possible mechanisms.

Table 3. Relative energies in kcal mol^{-1} of the stationary points of the indirect mechanisms for the (R,R) isomer of the PdHSS complex.

	(R,R)	$(R,R)^{EI}$
$TS1_{ID1}$	**15.0**	**n.c.**
$TS1_{ID1}$▲■	**17.8**	**20.5**
$TS1_{ID1}^{hs}$	**13.3**	**20.4**
$TS1_{ID2}$	**21.0**	**31.9**
$TS1_{ID2}$▲■	**18.2**	**30.6**
$I1_{ID1}$	10.8	n.c.
$I1_{ID1}$▲■	14.3	14.2
$I1_{ID1}^{hs}$	4.7	8.1
$I1_{ID2}$	10.2	11.4
$I1_{ID2}$▲■	7.9	11.5
$TS2_{ID1}$▲	**25.0**	**25.4**
$TS2_{ID1}$♦	**26.1**	**25.4**■
$TS2_{ID2}$	**22.7**	**24.8**
$TS2_{ID2}$■	**19.8**	**25.2**
$I2_{ID1}$▲	16.6	17.4
$I2_{ID1}$♦	20.1	19.1■
$I2_{ID2}$	18.2	16.7
$I2_{ID2}$■	15.6	19.0
$TS3_{ID1}$▲	**25.5**	**25.1**
$TS3_{ID1}$♦	**22.2**	**21.8**■
$TS3_{ID2}$	**21.2**	**21.1**
$TS3_{ID2}$■	**22.2**	**24.9**
P_{ID1}▲/■	-3.5	-4.8
P_{ID1}♦	-3.3	-2.7
P_{ID2}	-1.5	1.2
P_{ID2}■	-0.9	2.3

■ square motifs instead of a diamond
n.c. not calculated

In $I1_{ID1}$, the H-bond network is the same as the one in $I1_{D1}$. It has an N2–Pd–O1 angle of 133°, which is lowered to 103° in $TS2_{ID1}$▲ as the coordinated water is substituted by the hydrogen. The displaced solvent molecule pushes away the phenolate almost to the axial position creating a Pd–O1 separation of 306 pm. This effect can be bypassed if the dissociating water is inserted into the trigonal network in the same TS. In the ID1 approach, this yields $TS2_{ID1}$♦ (Fig. S30) where a diamond-shaped network of four H-bonds is created by three water molecules and O1, restoring the N2–Pd–O1 angle to 132°. This leads to a considerably longer Pd–O1 distance (395

pm) as well as slightly longer (~5 pm) Pd–H bonds which is the likely cause of an energy increase (26.1 kcal mol^{-1}) relative to $TS2_{ID1}$ (25.0 kcal mol^{-1}). The diamond-shape motif formed spontaneously during the study of proton transfer from the coordinated water molecule to the dissociated phenolate arm, and it appears only as a projection similar to the square motif, see Fig S30. In $I1_{ID1}$ the dissociated phenolate oxygen is very close to facilitate the formation of a hydroxo complex (P_{ID1}^{OH}) directly. Although the TS energy indicates a very fast deprotonation process, the hydroxo complex formation is strongly endergonic in contrast to the thermodynamically allowed monohydride product, see Fig. S31. As the hydroxide is less likely to be replaced by H_2, these species were not considered as intermediates in subsequent reaction steps.

3.8. Pd-H formation: Indirect route – the ID2 mechanism

In the case of the ID2 approach, the distal amino proton is facing towards the other side of the dissociated phenolate arm. $TS1_{ID2}$ has a chain orientation of oxygen atoms similar to the one in $TS1_{ID1}$. $TS1_{ID2}^{▲■}$ contains a triangle formed by O1, $O^{W1,}$ and N1, together with a square formed spontaneously by O1, O2, and two water oxygens as shown in Fig. S30. Hydroxo complex formation showed a more exergonic process in the case of $I1_{ID2}$ than for $I1_{ID1}$ (Fig. S31).

In ID2 there are also two kinds of TS2: one contains a square shape formed by O1 and water oxygens while the other has a triangle formed by O1 and two water oxygens. The latter can also rearrange to accommodate a different type of square pattern. During these transformations, a pseudo square shape could be observed in which the trigonal shape is broken to open the way for the third water molecule, see the left side in Fig. 7. Note that all H-bond networks were formed in models where the number of water molecules (2 or 3) determined the maximal and optimal number of H-bonds.

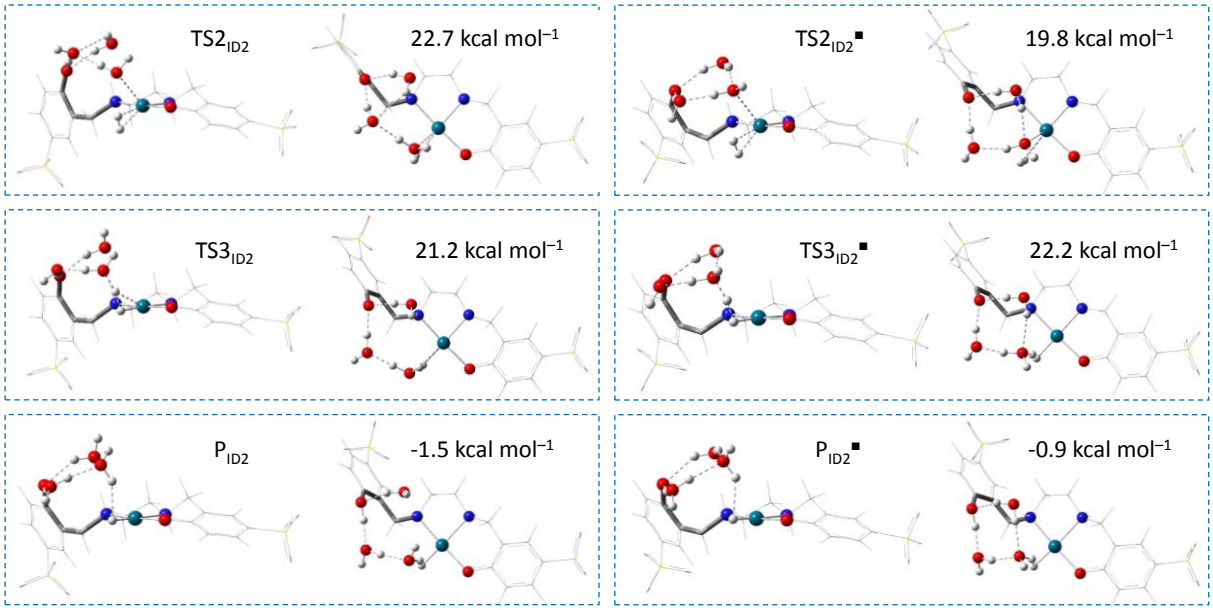

Figure 7. Optimized structures of TS2, TS3, and the product of both ID2 mechanisms in different orientations.

3.9. Comparing indirect routes: ID1 vs. ID2 mechanism

Comparison of ID1 and ID2 showed that in the second and third steps all stationary points had lower energy in ID2. Significant differences can be seen in TS2 where the $TS2_{ID2}$ forms were much more favored over $TS2_{ID1}$ excluding $(R,R)^{EI}$ which shows only a slight difference in activation energies of $TS2_{ID}$ forms. Table 3 shows that the substitution of water by hydrogen ($TS2_{ID2}$) and the proton transfer ($TS3_{ID2}$) have also relatively similar values.

Fig. 7 presents an energy profile in which the most preferred stationary points of (R,R) are shown from each mechanism. In the case of ID2, the two pathways can intercross each other due to the small differences in atomic orientations (Fig. 7) showing a preferred pathway through $TS2_{ID2}$■ and $TS3_{ID2}$. This intercross, however, cannot be considered for ID1 due to the very different atomic orientation of ♦ and ▲ pathways. Besides, we presume that an $I1_{ID1}$▲■ → $I1_{ID2}$▲■ interconversion may also occur to reach a more preferred orientation of ID2 for further steps. It can be described by the Pd–N–C7–C1 and N–C7–C1–C2 dihedral angles, and probably activation barriers are lower than that of substitution steps. (Of course, this statement is true for

the direct mechanism as well. As was discussed in the case of $(R,S)^{\delta}$, D2 went through a D1-type proton transfer step due to the orientation of the dissociated phenolate arm, see Fig. S13.)

3.10. Comparing the possible routes

Comparing the four mechanisms we can conclude that D1 and ID2 are competitive with each other: D1 is the most preferred (rate-determining step is at 20.0 kcal mol^{-1}), while the RDS of ID2 is somewhat higher (21.2 kcal mol^{-1}). It is worth mentioning that the products of the direct mechanisms are less favored thermodynamically. However, the products of the direct pathways (P_{D1} and P_{D2} in Figure 7) were derived from the products of ID processes by removing one water molecule, and re-optimizing them. For both D1 and D2 the re-optimized products are 2-3 kcal mol^{-1} lower in energy than the products derived directly from $TS2_{D1/D2}$, see Table S12. Note that P_{D1} in Figure 7 and the $P_{D1}{}^{W}$ included in Table 2 are identical. The different products found from different mechanisms show that an energy interval can be defined for the monohydride products due to the flexible protonated phenolate. Furthermore, it shows that the lowest barrier of the monohydride complex formation is belonging to the one that goes through the arm rotated species ($R_{D1}{}^{hs}$ in Fig. 8).

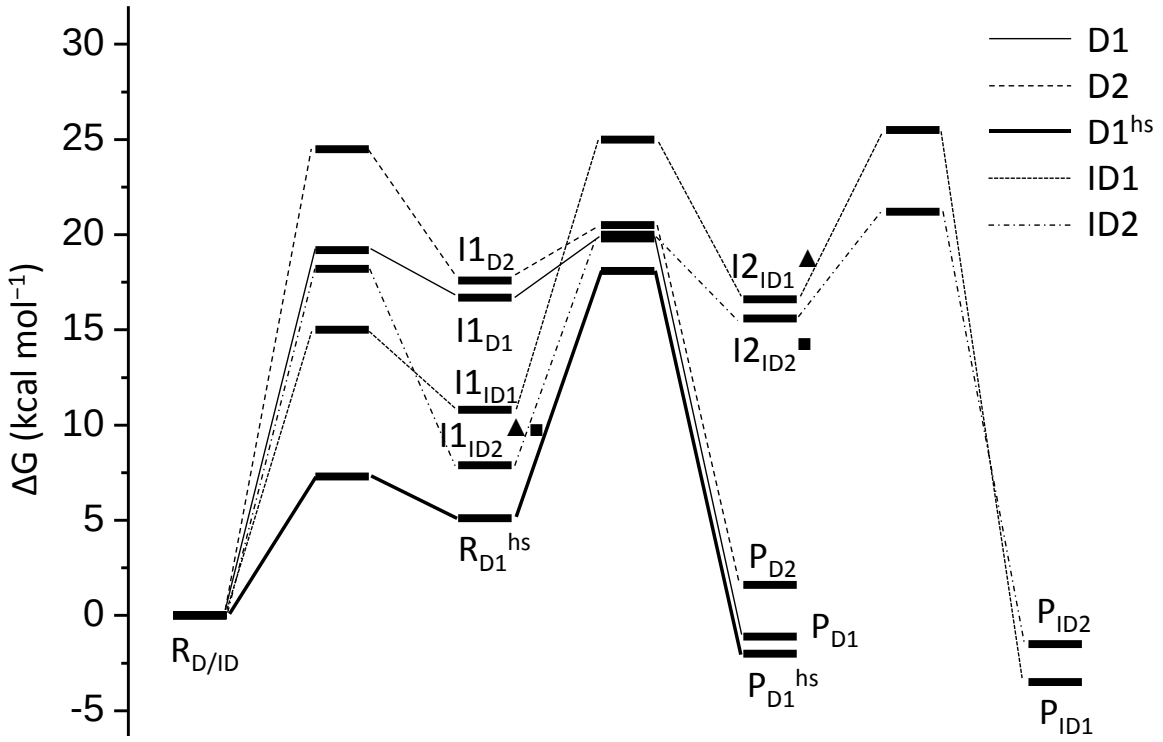

Figure 8. Energy profile of the mechanisms studied for the (R,R) isomer.

We did not find any huge effect of substituted derivatives, therefore, all information is discussed in SI in detail. We found, however; that the hydride formation of the salen complex is strongly endergonic, and only the direct mechanism could be found, see the Supplementary Material for the details. It was found that the monohydride products of Pd-salen are ~10 kcal mol^{-1} higher but activation energies are only ~4 kcal mol^{-1} higher in energy. This evidence is based on the rigid-flexible relation of the salen and salan complexes.

Comparing these results with reports by other groups is difficult as not many similar works that employ computations are available. Hou et al. investigated hydride formation in Co, Rh and Ir complexes with a non-flexible bipyridine ligand [41]. They found that proton transfer from the coordinated hydrogen can take place through a water channel with activation energies of 18.3 kcal mol^{-1}, 14.2 kcal mol^{-1}, and 13.4 kcal mol^{-1} for the three metals, respectively. They propose an indirect mechanism where the reference structure contains a coordinated water molecule like

in the $I1_{ID2}$ form discussed here. The most significant difference is that in their complex, the oxygen atoms of the ligand are non-coordinating, whereas, in the case of salan, they are. Also, they did not account for water-hydrogen substitution, which step has a barrier comparable to that of the proton transfer. We also compared the energies of the ID mechanism of PdHSS described here with those of the Rh-bipyridine complex in Ref. 41 due to the similar metal size. The activation barrier of proton transfer concerning the water-coordinated state $I1_{ID2}$ is 14.3 kcal mol^{-1} (the energy difference of $I1_{ID2}$▲■ and $TS3_{ID2}$■), essentially the same as the value of 14.2 kcal mol^{-1} reported by Hou et al. Note that the definition of the reactant states is different in the two works. As we find that $I1_{ID2}$ is a high energy intermediate, the two approaches yield different barriers and reaction free energies for the overall reactions. It also means that the free energy of hydride complex formation from $I1_{ID2}$ is considerably lower for PdHSS (-4.8 in Ref. 41 vs. -8.8 kcal mol^{-1}—the energy difference of $I1_{ID2}$▲■ and $TS3_{ID2}$■—here), indicating a more endergonic process. The Pd-salan complex, however, offers pathways with barriers lower than the one calculated for the ID2 mechanism. These additional pathways start from the different initial PdHSS isomers (Figs. 2-3) that are connected by intramolecular arm rotation. It emphasizes the importance of ligand flexibility in the hydride formation reaction, which probably can be extended to other reactions such as redox isomerization [15].

4. Conclusion

In this work, we studied the reaction between hydrogen and the PdHSS complex to develop a mechanism that explains the effect of ligand flexibility on hydride complex formation. The flexibility of the salan ligand implies that several accessible PdHSS isomers can initiate the process. These species are connected by the rotation of the phenolate arm and the inversion of the ethylene backbone as both involve relatively low barriers. Two main mechanistic approaches were considered: One is the direct monohydride formation in which at first the

phenolate arm was substituted by hydrogen. The other, indirect one involves a preceding solvent (water) coordination. Among the two, the direct mechanism is preferred but the most favored path is the one starting from the half stepped conformer in which one of the phenolate arms is rotated by an intramolecular rearrangement. Various arrangements of hydrogen bond networks were formed spontaneously by two or three water molecules, oxygen atoms of the phenolate groups, and the –NH groups. Trigonal motif appeared during the proton transfer step of the preferred direct mechanism, however, in some cases square or trigonal and square motifs together showed relevance, while diamond-shape motif was not favored.

Experimentally we found a hydride signal which was assigned as a monohydride compared to the simulated NMR spectra. UV-Vis spectra supported these findings since the monohydride showed almost the same spectrum but with lower intensity.

On the one hand, we studied minor pathways such as H-transfer to the phenolic ring or dihydride formation, which were not relevant because of the (very) high activation barriers. On the other hand, Pd(0) complexes were found when the hydride ligand is formally transferred to the coordinated amino group as a proton. These Pd(0) complexes can then undergo a favorable dimerization.

We found that monohydride formation from the palladium-salen complex was strongly endergonic due to the stretching of the dissociated arm having an imine group in contrast to salan complexes which are mostly exergonic. Activation barriers were also somewhat higher than for the salan complex. Hydroxo complex formation was also strongly endergonic for both salen and salan complexes which does not hinder the hydride formation.

In conclusion, the preference of the intramolecular rotation and the diversity of possible pathways all result from the flexibility of the salan ligand.

Associated content

Appendix A. Supplementary Material

Supplementary data associated with this article can be found, in the online version, at

Corresponding author

Mihály Purgel – *Department of Physical Chemistry, University of Debrecen, Egyetem tér 1, H-4032 Debrecen, Hungary;* orcid.org/0000-0002-9982-8590; Email: purgel.mihaly@science.unideb.hu

Notes

The authors declare no competing financial interest.

Acknowledgment

This work was partially supported by the European Union and the European Social Fund through project Supercomputer, the National Virtual Lab, grant no.: TÁMOP-4.2.2.C-11/1/KONV-2012-0010. The research was supported by the EU and co-financed by the European Regional Development Fund under the project GINOP-2.3.2-15-2016-00008 and GINOP-2.3.3-15-2016-00004. Special thanks to Dr. Antal Udvardy for the help with the NMR measurements.

References

[1] Cubillos J.; Montilla I.; Montes de Correa C. Easy separation and reutilization of the Jacobsen's catalyst in olefin oxidation. *Applied Catalysis A: General* **2009,** *366,* 348–352.

[2] Cubillos J.; Vásquez S.; Montes de Correa C. Salen manganese (III) complexes as catalysts for R-(+)-limonene oxidation. *Applied Catalysis A: General* **2010,** *373,* 57–65.

[3] Jang, D.; Lee, Y.; Shin, Y.; Park, S.; Jo, C.; Kim, Y. H.; Park, S. Coordination structure of Jacobsen catalyst with N-modified graphene and their electrocatalytic properties for reducing oxygen molecules. *Applied Catalysis B: Environmental* **2020,** *263,* 118337–118345.

[4] Mohan, N.; Sreejith, S. S.; Prathapachandra Kurup, M. R. Investigation on catecholase activity of salen Co(III) octahedral complexes. *Polyhedron* **2019,** *173,* 114129–114137.

[5] Gutierrez, K.; Corchado, J.; Lin, S.; Chen, Z.; Piñero Cruz, D. M. A non-innocent salen naphthalene ligand and its Co^{2+}, Ni^{2+} and Cu^{2+} metal complexes: Structural, electrochemical, and spectroscopic characterization and computational studies. *Inorg. Chim. Acta* **2018,** *474,* 118–127.

[6] Blanchard, R.; Martin, V.; Mantoux, A.; Chatenet, M. Cobalt porphyrin and salcomine as novel redox shuttle species to enhance the Oxygen Evolution Reaction in Li-O2 batteries. *Electrochimica Acta* **2018,** *261,* 384–393.

[7] Takizawa, N.; Kimura, T.; Watanabe, T.; Shibasaki, M. Anti‐influenza virus activity of a salcomine derivative mediated by inhibition of viral RNA synthesis. *Arch Virol.* **2018,** *163,* 1607–1614.

[8] Adão P.; Barroso S.; Avecilla F.; Conceição Oliveira M.; Costa Pessoa J. Cu^{II}–salan compounds: Synthesis, characterization and evaluation of their potential as oxidation catalysts. *Journal of Organometallic Chemistry* **2014,** *760,* 212–223.

[9] Benferrah N.; Hammadi M.; Philouze C.; Berthiol F.; Thomas F. Copper(II) complex of a Schiff base of dehydroacetic acid: Characterization and aerobic oxidation of benzyl alcohol. *Inorg. Chem. Comm.* **2016,** *72,* 17–22.

[10] Ayala V.; Corma A.; Iglesias M.; Rincón J.A.; Sánchez F. Hybrid organic—inorganic catalysts: a cooperative effect between support, and palladium and nickel salen complexes on catalytic hydrogenation of imines. *J. Catal.* **2004,** *224,* 170.

[11] Liu P.; Feng X.-J.; He R. Salen and half-salen palladium(II) complexes: synthesis, characterization and catalytic activity toward Suzuki–Miyaura reaction. *Tetrahedron* **2010,** *66,* 631–636.

[12] Liu Y.-S.; Gu N.-N.; Liu P.; Ma X.-W.; Liu Y.; Xie J.-W.; Dai B. Water-soluble salen-Pd complex as an efficient catalyst for Suzuki-Miyaura reaction of sterically hindered substrates in pure water. *Tetrahedron* **2015,** *71,* 7985–7989.

[13] Heo Y.; Kang Y. Y.; Palani T.; Lee J.; Lee S. Synthesis, characterization of palladium hydroxysalen complex and its application in the coupling reaction of arylboronic acids: Mizoroki–Heck type reaction and decarboxylative couplings. *Inorg. Chem. Comm.* **2012,** *23,* 1–5.

[14] Yuan L.; Xu Y.; Hu X.; Yang G.; Wu Y. A water-soluble palladium-salen catalyst modified by pyridinium salt showing higher reactivity and recoverability for Heck coupling reaction. *J. Mol. Cat. A: Chemical* **2015,** *396,* 55–60.

[15] Voronova K.; Purgel M.; Udvardy A.; Bényei A. C.; Kathó Á.; Joó F. Hydrogenation and Redox Isomerization of Allylic Alcohols Catalyzed by a New Water-Soluble Pd−tetrahydrosalen Complex. *Organometallics*, **2013**, 32, 4391–4401.

[16] Gombos, R.; Nagyházi, B.; Joó, F. Hydrogenation of α,β‐unsaturated aldehydes in aqueous media with a water‐soluble Pd(II)‐sulfosalan complex catalyst. *React. Kinet. Mech. Cat.* **2019,** *126,* 439–451.

[17] Voronova K.; Homolya L.; Udvardy A.; Bényei A. C.; Joó F. Pd–Tetrahydrosalan-Type Complexes as Catalysts for Sonogashira Couplings in Water: Efficient Greening of the Procedure. *ChemSusChem*. **2014,** *7,* 2230–2239.

[18] Bunda, S.; Udvardy, A.; Voronova, K.; Joo, F. Organic solvent-free, Pd(II)-salan complex-catalyzed synthesis of biaryls via Suzuki-Miyaura cross-coupling in water and air. *J. Org. Chem.* **2018,** *83,* 15486–15492.

[19] Pessoa, J. C.; Correia I. Salan vs. salen metal complexes in catalysis and medicinal applications: Virtues and pitfalls. *Coord. Chem. Rev.* **2019,** *388,* 227–247.

[20] Clarke, R. M.; Herasymchuk, K.; Storr T. Electronic structure elucidation in oxidized metal–salen complexes. *Coord. Chem. Rev.* **2017,** *352,* 67–82.

[21] Kokubo, C.; Katsuki T. Highly Enantioselective Catalytic Oxidation of Alkyl Aryl Sulfides Using Mn-Salen Catalyst. *Tetrahedron,* **1996,** *52,* 13895–13900.

[22] Palucki, M.; Hanson, P.; Jacobsen E. N. Asymmetric Oxidation of Sulfides with H_2O_2 Catalyzed by (salen)Mn(III) Complexes. *Tetrahedron Letters.* **1992,** *33,* 7111–7114.

[23] Peri, D.; Meker, S.; Manna, C. M.; Tshuva E. Y. Different ortho and para Electronic Effects on Hydrolysis and Cytotoxicity of Diamino Bis(Phenolato) "Salan" Ti(IV) Complexes. *Inorg. Chem.* **2011,** *50,* 1030–1038.

[24] Matsumoto, K.; Sawada, Y.; Saito, B.; Sakai, K.; Katsuki, T. Construction of Pseudo-Heterochiral and Homochiral Di-m-oxotitanium(Schiff base) Dimers and Enantioselective Epoxidation Using Aqueous Hydrogen Peroxide. *Angew. Chem. Int. Ed.* **2005,** *44,* 4935–4939.

[25] Zhang, G. A heterotrimetallic Pd–Sm–Pd complex for asymmetric Friedel–Crafts alkylations of pyrroles with nitroalkenes. *Org. Biomol. Chem.,* **2012,** *10,* 2534–2536.

[26] Adão, P.; Maurya, M. R.; Kumar, U.; Avecilla, F.; Henriques, R. T.; Kusnetsov, M. L.; Pessoa, J. C.; Correia, I. Vanadium-salen and -salan complexes: Characterization and application in oxygentransfer reactions. *Pure Appl. Chem.*, **2009,** 81, 1279–1296.

[27] Cozzolino, M.; Leo, V.; Tedesco, C.; Mazzeo, M.; Lamberti, M. Salen, Salan and Salalen Iron (III) Complexes as Catalysts for CO2/Epoxides Reactions and ROP of Cyclic Esters. *Dalton Trans.,* **2018,** *47,* 13229–13238.

[28] Parr, R. G.; Yang, W. *Density Functional Theory of Atoms and Molecules;* Oxford University Press: New York, USA, 1989.

[29] Gaussian 09, Revision **E.01**, M. J. Frisch, G. W. Trucks, H. B. Schlegel, G. E. Scuseria, M. A. Robb, J. R. Cheeseman, G. Scalmani, V. Barone, B. Mennucci, G. A. Petersson, H. Nakatsuji, M. Caricato, X. Li, H. P. Hratchian, A. F. Izmaylov, J. Bloino, G. Zheng, J. L. Sonnenberg, M. Hada, M. Ehara, K. Toyota, R. Fukuda, J. Hasegawa, M. Ishida, T. Nakajima, Y. Honda, O. Kitao, H. Nakai, T. Vreven, J. A. Montgomery, Jr., J. E. Peralta, F. Ogliaro, M. Bearpark, J. J. Heyd, E. Brothers, K. N. Kudin, V. N. Staroverov, R. Kobayashi, J. Normand, K. Raghavachari, A. Rendell, J. C. Burant, S. S. Iyengar, J. Tomasi, M. Cossi, N. Rega, J. M. Millam, M. Klene, J. E. Knox, J. B. Cross, V. Bakken, C. Adamo, J. Jaramillo, R. Gomperts, R. E. Stratmann, O. Yazyev, A. J. Austin, R. Cammi, C. Pomelli, J. W. Ochterski, R. L. Martin, K. Morokuma, V. G. Zakrzewski, G. A. Voth, P. Salvador, J. J. Dannenberg, S. Dapprich, A. D. Daniels, Ö. Farkas, J. B. Foresman, J. V. Ortiz, J. Cioslowski, and D. J. Fox, *Gaussian, Inc.*, Wallingford CT, **2009**

[30] Zhao Y.; Truhlar D. G. The M06 suite of density functionals for main group thermochemistry, thermochemical kinetics, noncovalent interactions, excited states, and transition elements: two new functionals and systematic testing of four M06-class functionals and 12 other functionals. *Theor. Chem. Acc.* **2008,** *120,* 215–241.

[31] Andrae D.; Haeussermann U.; Dolg M.; Stoll H.; Preuss H. Energy-adjusted ab initio pseudopotentials for the second and third row transition elements. *Theor. Chim. Acta* **1990,** *77,* 123–141.

[32] Schaefer A.; Horn H.; Ahlrichs R. Fully optimized contracted Gaussian-basis sets for atoms Li to Kr. *J. Chem. Phys.* **1992,** *97,* 2571–2577.

[33] Schaefer A.; Huber C.; Ahlrichs R. Fully optimized contracted Gaussian-basis sets of triple zeta valence quality for atoms Li to Kr. *J. Chem. Phys.* **1994,** *100,* 5829–5835.

[34] Miertuš S.; Scrocco E.; Tomasi J. Electrostatic Interaction of a Solute with a Continuum. A Direct Utilization of ab initio Molecular Potentials for the Prevision of Solvent Effects. *Chem. Phys.* **1981**, *55*, 117–29.

[35] Purgel M.; Platas-Iglesias C.; de Blas A.; Rodríguez-Blas T.; Baranyai Z.; Bányai I.; Tóth I. An NMR and DFT Investigation on the Conformational Properties of Lanthanide(III) 1,4,7,10-Tetraazacyclododecane-1,4,7,10-tetraacetate Analogues Containing Methylenephosphonate Pendant Arms, *Inorg. Chem*. **2010,** *49*, 4370–4382.

[36] Cozzi, P. G. Metal–Salen Schiff base complexes in catalysis: practical aspects. *Chem. Soc. Rev.* **2004,** *33*, 410–421.

[37] Nworie, F. S. Bis(Salicylidene) Ethylenediamine(Salen) and Bis(Salicylidene) Ethylenediamine-Metal Complexes: from Structure to Biological Activity. *J. Anal. Pharm. Res.* **2016,** *3*, 76–85.

[38] Smelova, K. M.; Bazhanov, D. I.; Stepanyuk, V. S.; Hergert, W.; Saletsky, A. M.; Bruno P. Interplay between magnetism and structure in atomic-size Pd contacts: Ab initio studies. *Phys. Rev. B* **2008,** *77*, 033408.

[39] Tsysar, K. M.; Bazhanov, D. I.; Saletsky, A. M.; Stepanyuk, V. S.; Hergert, W. Effect of Hydrogen Impurity Atoms and Molecules on the Atomic Structure of Palladium Nanocontacts. *Phys. Solid State*, **2010,** *52*, 641–648.

[40] Wierzbowska, M.; Delin, A.; Tosatti, E. Effect of electron correlations in Pd, Ni, and Co monowires. *Phys. Rev. B* **2005,** *72*, 035439.

[41] Hou, C.; Jiang, J.; Zhang, S.; Wang, G.; Zhang, Z.; Ke, Z.; Zhao, C. Hydrogenation of Carbon Dioxide Using Half-Sandwich Cobalt, Rhodium, and Iridium Complexes: DFT Study on the Mechanism and Metal Effect. *ACS Catalysis*, **2014,** *4*, 2990–2997.